Dynamical Properties of Polymer Solutions in Good Solvent by Rayleigh Scattering Experiments

M. Adam* and M. Delsanti*

Commissariat a L'Energie Atomique, Division de la Physique, Service de Physique du Solide et de Resonance Magnetique, 91190 Gif-sur-Yvette, France. *Received March 25, 1977*

ABSTRACT: We present experimental data on the dynamical behavior of polymer (polystyrene) solutions in good solvent. The technique used is intensity-fluctuation spectroscopy, which allows us to determine the characteristic time of the dynamical structure factor of the polymer. The dynamical response of the polymer is given as a function of wave vector **K**, concentration c, and molecular weight M. We determine three dynamical exponents α, β, and γ: (1) In dilute solution, the hydrodynamical radius of the polymer increases with the molecular weight as M^{α} where $\alpha = 0.55 \pm 0.02$. We found experimentally that the geometrical radius scales as M^{ν} where ν is the static exponent equal to 0.6. (2) At concentrations where polymer chains overlap the solutions behave like gels of finite lifetime. The cooperative diffusion coefficient depends on concentration only and increases with concentration as c^{β} where $\beta = 0.67 \pm 0.02$. (3) In dilute solution, at wave vector **K** greater than R^{-1}, where R is the coil radius of gyration ($\mathbf{K}R \geq 4.4$), the inverse characteristic time depends only on **K** and increases as $\mathbf{K}^{\gamma}$ where $\gamma = 2.85 \pm 0.05$. These experimental data are compared to the exponent values and scaling laws proposed recently by de Gennes. The main assumption of de Gennes' calculation is that static and dynamical lengths are identical. This is not verified experimentally but the exponents α, β, and γ measured are self-consistent and connected by the scaling laws: $\alpha = (3\nu - 1)\beta$, $\gamma = 2 + \alpha/\nu$.

The conformation of macromolecules in good solvent has been studied both experimentally and theoretically[1] in dilute and semidilute solutions. We shall first recall some of the concepts and methods used for the determination of spatial properties of polymers because they will be of importance in the derivation of dynamical properties.

At very low monomer concentration c (dilute solution), the macromolecules behave like a collection of independent coils with a geometrical size R (radius of gyration) given by:

$$R = a(M/m)^{\nu} \qquad (\nu = 0.6) \tag{1}$$

a is the length and m the molecular weight associated with the statistical element, and M is the molecular weight of the macromolecule. The macromolecules begin to overlap at concentration c^* such that the distance between the centers of two neighboring coils is equal to $2R$:

$$c^* = \frac{M}{R^3} = \frac{m}{a^3}(M/m)^{(1-3\nu)} \qquad [(1 - 3\nu) = -0.8] \tag{2}$$

When the concentration is larger than c^* (semidilute solution) the polymer chains have contact points and the spatial monomer distribution is homogeneous. Then the average distance between adjacent contact points, ξ, is independent of the polymer weight and varies with concentration as $c^{\nu/(1-3\nu)}$ ($= c^{-0.75}$). This last point can be obtained by a scaling law. Assuming that the length ξ behaves like some power of the concentration and that ξ and R must have the same order of magnitude at the transition between dilute and semidilute regime (c^*) we derive:

$$\xi = R(c/c^*)^{\nu/(1-3\nu)} \tag{3}$$

The important result obtained in recent studies of polymer configuration is that ξ is also the distance beyond which excluded volume effects are screened out.

These views have been extended recently to time-dependent properties by de Gennes[2] and have stimulated us to study the dynamical properties of polymer. We present here quasielastic Rayleigh light-scattering experiments which allow us to measure the following dynamical structure factor

$$S(\mathbf{K},t) = \langle \delta C(\mathbf{K},t)\delta C^{+}(\mathbf{K},0)\rangle \tag{4}$$

where $\delta C(\mathbf{K},t)$ is the spatial Fourier transform of the local monomer concentration fluctuations at time t and for a momentum transfer **K** of the scattered light.

Part I of this paper contains a general presentation of different dynamical regimes which can be accessible by quasielastic light-scattering experiment. The experimental procedure is described in part II. Part III is concerned with the presentation and discussion of the results of our study of the dynamical structure factor for solutions of polystyrene in benzene at room temperature. The behavior of the characteristic times at the boundaries between the various regimes is examined in part IV.

I. Dynamical Regimes

To investigate the different dynamical regimes it is useful to define two parameters: the reduced concentration c/c^* and the dimensionless quantity $\mathbf{K}L$, where L is the characteristic length of the system

$$\begin{aligned} L &= R \text{ in dilute regime} && c/c^* < 1 \\ L &= \xi \text{ in semidilute regime} && c/c^* > 1 \end{aligned} \tag{I.1}$$

At a given momentum transfer **K**, the light scattered reflects length correlations of order $\mathbf{K}^{-1}$. At $\mathbf{K}L \ll 1$, we have access to macroscopic properties, whereas at $\mathbf{K}L \gg 1$ the scattering is related to "local" properties (i.e., internal motions of the polymer chain). These two regions are schematically represented in the plane $\mathbf{K}R$ vs. c/c^* (Figure 1), where the upper full line corresponds to $\mathbf{K}_{max}L = 1$. With the explicit expression of ξ (eq 3) and the exponent value $\nu = 0.6$ we find that:

$$\begin{aligned} \mathbf{K}_{max} &= r^{-1} \text{ at } c/c^* < 1 \\ \mathbf{K}_{max} &= R^{-1}(c/c^*)^{0.75} \text{ at } c/c^* > 1 \end{aligned} \tag{I.2}$$

(1) Characteristic Times in the Lower Momentum Range $\mathbf{K}L \ll 1$. (a) Dilute Solutions (Region 1 in Figure 1). In this region polymer chains are well separated and act as entities. By quasielastic light scattering at **K** vector such that $\mathbf{K}R \ll 1$, we observe the Brownian motion of the whole macromolecule. The dynamical structure factor has the well-known form:[3]

$$S(\mathbf{K},t) = S(\mathbf{K},0)e^{-D_0\mathbf{K}^2 t} \tag{I.3}$$

where D_0 is the translational diffusion coefficient of the chain in the limit $c = 0$. Assuming the validity of Stokes law and using the Einstein relation, we have:

$$D_0 = \mathbf{K}_B T/6\pi\eta R \tag{I.4}$$

if we suppose that *the hydrodynamical radius is equal to the*

radius of gyration. $\mathbf{K}_B$ is the Boltzman constant, T is the temperature, and η is the solvent viscosity. This leads to the following molecular weight dependence:

$$D_0(M) = \frac{\mathbf{K}_B T}{6\pi\eta a}\left(\frac{M}{m}\right)^{-\nu} \tag{I.5}$$

(b) Semidilute Solution: "Pseudo-Gel Domain" (Region 2 in Figure 1). In this domain de Gennes[2] argues that the entangled polymer solutions behave like polymer networks swollen by the solvent. The spatial Fourier transform of the longitudinal displacements of the polymer network has the following time dependence:

$$u(\mathbf{K},t) = u(\mathbf{K},0)e^{-(E/f)\mathbf{K}^2 t} \tag{I.6}$$

where E is the elastic modulus of the polymer network and f is the friction per unit volume between the solvent and the polymer. This is similar to the results obtained in a gel with permanent cross-links.[4] The classical theory[5] of rubber elasticity specifies that the elastic modulus is proportional to the volume number density of strands n:

$$E = n\mathbf{K}_B T \tag{I.7}$$

In our case the fibers of the network have a mean length equal to ξ so $n = 1/\xi^3$ and we can estimate that:

$$E = \mathbf{K}_B T/\xi^3 \tag{I.8}$$

The friction coefficient per unit volume is expressed as

$$f = 6\pi\eta\xi_H/\xi^3 \tag{I.9}$$

where ξ_H is the hydrodynamical length associated with the monomers contained in a volume ξ^3. With formulas I.8 and I.9 we derive the displacement:

$$u(\mathbf{K},t) = u(\mathbf{K},0)e^{-D_g\mathbf{K}^2 t} \tag{I.10}$$

with

$$D_g = \mathbf{K}_B T/6\pi\xi_H$$

de Gennes shows that *the hydrodynamical length* ξ_H *is identical with the screening length* ξ defined in eq 3. With the explicit expression of ξ we obtain

$$D_g(c) = \frac{\mathbf{K}_B T}{6\pi R}\left(\frac{c}{c^*}\right)^{\nu/(3\nu-1)} \sim c^{0.75} \tag{I.11}$$

Let us note at this point that, like the spatial properties,[18] the concentration dependence of $D_g(c)$ can also be obtained by a scaling assumption:

$$D_g(c) = D_0(M)(c/c^*)^m \tag{I.12}$$

The power m is determined from the assumption that the diffusion coefficient $D_g(c)$ is independent of molecular weight. From eq 2 and I.5 for c^* and D_0 it follows that $m = \nu/(3\nu - 1) = 0.75$.

The contact points of the polymer network have a finite lifetime, T_R:

$$T_R = \frac{6\pi\eta}{\mathbf{K}_B T} R^3 \left(\frac{c}{c^*}\right)^{3(1-\nu)/(3\nu-1)} \tag{I.13}$$

The gel picture has a meaning only when the characteristic time $\tau(\mathbf{K}) = (D_g(c)K^2)^{-1}$ is shorter than T_R. With the expression of $\tau(\mathbf{K})$ and T_R the wave vector range for which this condition is respected is

$$\mathbf{K} \geq \mathbf{K}_{min} = R^{-1}(c/c^*)^{-1.125} \tag{I.14}$$

In the plane $\mathbf{K}R$ vs. c/c^* (Figure 1) the value $\mathbf{K}_{min}$ corresponds to the dashed line.

At the $\mathbf{K}$ vectors investigated a semidilute solution can be treated as a continuous medium and concentration fluctuations $\delta C(\mathbf{K},t)$ are proportional to the longitudinal displacements $u(\mathbf{K},t)$. The dynamical structure factor is

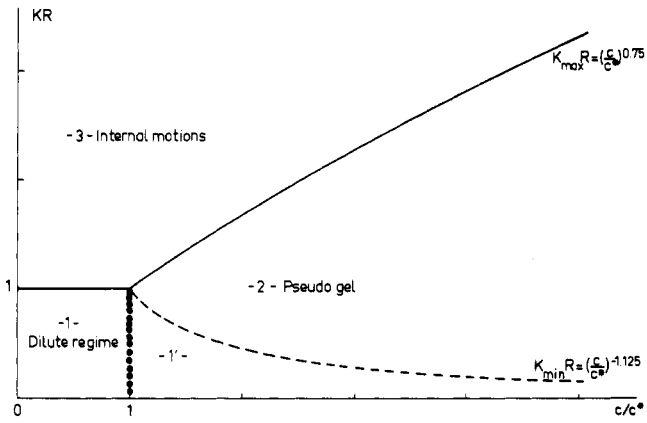

Figure 1. Schematic diagram of the different dynamical regimes.

$$S(\mathbf{K},t) = S(\mathbf{K},0)e^{-D_g(c)K^2 t} \tag{I.15}$$

(2) Characteristic Time in the Upper Momentum Range $\mathbf{K}L \gg 1$ (Region 3 in Figure 1). Light-scattering experiments measure the dynamical structure factor:[6]

$$S(\mathbf{K},t) \simeq \sum_{ij} \langle e^{-i\mathbf{K}(r_i(t)-r_j(0))}\rangle \tag{I.16}$$

where $r_i(t)$, $r_j(0)$ are the positions of the ith and jth monomers at times t and 0, respectively. At $\mathbf{K}L \gg 1$ the dynamical structure factor reflects properties of the polymer chain on distances smaller than L. The characteristic time, derived by a scaling argument,[2] has the form:

$$\tau^{-1}(\mathbf{K}) = D\mathbf{K}^2(\mathbf{K}L)^p \tag{I.17}$$

where D is the diffusion coefficient of the coil in dilute range ($D = D_0(M)$) and the cooperative diffusion in semidilute range ($D = D_g(c)$). In each case assuming the validity of Stokes law, de Gennes derives:

$$D = \mathbf{K}_B T/6\pi\eta L \tag{I.18}$$

At $\mathbf{K}L \gg 1$, the inverse characteristic time is related to local properties and must be $\mathbf{K}$ dependent only, therefore $p = 1$ and

$$\tau^{-1}(\mathbf{K}) = \frac{\mathbf{K}_B T}{6\pi\eta}\mathbf{K}^3 \tag{I.19}$$

This result is independent of the exponent value ν and is in agreement with previous results found for an infinite ideal coil by a microscopical approach.[7] Taking into account hydrodynamic interactions between monomer the following results have been derived:

$$S(\mathbf{K},t) = S(\mathbf{K},0)G(\tau^{-1}(\mathbf{K})t) \tag{I.20}$$

where G is not an exponential function of time but the sum

$$G(t\tau^{-1}(\mathbf{K})) = (t\tau^{-1}(\mathbf{K}))^{2/3}\int_0^\infty du \times \exp(-(t\tau^{-1}(\mathbf{K}))^{2/3}u(1 + h(u))) \tag{I.21}$$

with

$$h(u) = \frac{4}{\pi}\int_0^\infty \frac{dy \cos y^2}{y^3}[1 - \exp(-y^3u^{-3/2})]$$

The inverse characteristic time is

$$\tau^{-1}(\mathbf{K}) = \frac{1}{2^{3/2}3\pi}\frac{\mathbf{K}_B T}{\eta}\mathbf{K}^3 \tag{I.22}$$

Table I
Summary of Theoretical Predictions, with Hydrodynamical Interactions

	$c/c^* \ll 1$	$c/c^* \gg 1$
$\mathbf{K}L \ll 1$	$\tau^{-1} \sim M^{-0.6}\mathbf{K}^2$	$\tau^{-1} \sim c^{0.75}\mathbf{K}^2$
$\mathbf{K}L \gg 1$	$\tau^{-1} \sim \mathbf{K}^3$	

Now let us note that the **K** dependence on the characteristic time can be found by an intuitive argument. At a given momentum transfer **K** we have access to the properties on distances of the order $\mathbf{K}^{-1}$. Assuming the validity of Stokes law for a sphere of size $\mathbf{K}^{-1}$ the corresponding diffusion coefficient is

$$D(\mathbf{K}) = \mathbf{K}_B T/6\pi\eta\mathbf{K}^{-1} \qquad \text{(I.23)}$$

If we suppose that $\tau^{-1} = D(\mathbf{K})\mathbf{K}^2$ we get expression I.19.

In short the theory predicts that the characteristic time of the dynamical structure factor varies continuously with **K** and c. At low momentum transfer ($\mathbf{K}L \ll 1$) and increasing the concentration we can observe successively: the diffusion of the coil and the cooperative diffusion of the polymer network. Increasing the momentum transfer we have access to internal motions of the chain. The different predictions are summarized in Table I.

II. Experimental Technique

(1) Quasielastic Light-Scattering Experiment. (a) General. The temporal dependence of the electric field $E_{\mathbf{K}}(X,t)$ of the light scattered at a point X far from the scattering volume is given by:[8]

$$E_{\mathbf{K}}(X,t) = bI_0^{1/2}\delta C(\mathbf{K},t)e^{-i\omega_0 t + i\varphi} \qquad \text{(II.1)}$$

where b is a time-independent parameter and φ is a constant phase. ω_0 and I_0 are respectively the frequency and the optical intensity of the incident radiation. $\delta C(\mathbf{K},t)$ is the Kth component of the Fourier transform of concentration fluctuations. The wave vector **K** is equal to the momentum transfer which is related to the scattering angle θ by the Bragg relation:

$$\mathbf{K} = (4\pi/\lambda_0)n \sin\theta/2 \qquad \text{(II.2)}$$

λ_0 is the wavelength of the incident beam and n is the refractive index of the medium.

By a variation of θ from 1 to 180° ($\lambda_0 = 4880$ Å, $n \simeq 1.5$), we cover the corresponding momentum range

$$3 \times 10^3 \text{ cm}^{-1} < \mathbf{K} < 4 \times 10^5 \text{ cm}^{-1}$$

This **K** range allows us to investigate the different dynamical properties of the polymer solutions which have been presented in part I. For instance, for a polymer of molecular weight 10^7 daltons in dilute solution at small angles we have access to the diffusion of the polymer coils; at large angle ($\theta > 14°$) we can measure the internal motions of the polymer chain.

The time relaxation of concentration fluctuations is studied by measuring the autocorrelation function of the scattered field, $\langle E_{\mathbf{K}}(t)E_{\mathbf{K}}^+(0)\rangle$, by intensity fluctuation spectroscopy. The principle of this technique can be briefly described as follows. The scattered field, $E_{\mathbf{K}}(t)$, at a momentum transfer **K** falls on the photocathode of the photomultiplier detector. At the moment, we observe the scattered field on a point of the photocathode and the variable X drops from our notation. As a photomultiplier is a square-law detector, the output signal is proportional to the instantaneous optical intensity $I_{\mathbf{K}}(t) = |E_{\mathbf{K}}(t)|^2$. The autocorrelation of the output signal of the photomultiplier is built up[9] by a correlator

$$S_{\text{exp}}(\mathbf{K},t) \sim \langle I_{\mathbf{K}}(t)I_{\mathbf{K}}(0)\rangle \text{ for } t \neq 0 \qquad \text{(II.3)}$$

If the scattered field obeys Gaussian statistics we have a relation between second-order correlation and autocorrelation:[9]

$$\langle I_{\mathbf{K}}(t)I_{\mathbf{K}}(0)\rangle = \langle I\rangle^2 + |\langle E_{\mathbf{K}}^+(t)E_{\mathbf{K}}(0)\rangle|^2 \qquad \text{(II.4)}$$

Taking the expression of the scattered field we find that the experimental autocorrelation is related to the dynamical structure factor by:

$$S^0_{\text{exp}}(\mathbf{K},t) = A_0 + B_0|S(\mathbf{K},t)|^2 \qquad \text{(II.5)}$$

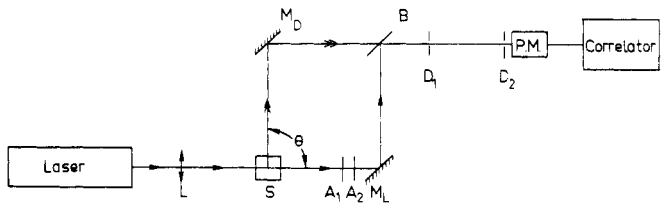

Figure 2. Block diagram of the spectrometer: S = sample; θ = scattering angle; L = lens; A_1, A_2 = polarizers; M_D, M_L = mirrors; B = beam splitter; and D_1, D_2 = diaphragms.

where A_0 and B_0 are two time-independent parameters. The experimental technique developed above is designated as homodyne detection.

Another experimental approach is the heterodyne detection. The scattered field is mixed at the photocathode with an additional monochromatic field, E_L, of large and constant intensity I_L, which acts as a local oscillator:

$$E_L = I_L^{1/2}e^{-i\omega_0 t + i\varphi} \qquad \text{(II.6)}$$

The spatial matching of fields must be perfect, i.e., the plane waves and the polarization of the two fields must coincide. The instantaneous intensity at the photocathode is:

$$I(t) = I_L + I_0 b^2|\delta C(\mathbf{K},t)|^2 + b(I_L I_0)^{1/2}(\delta C(\mathbf{K},t) + \delta C^+(\mathbf{K},t)) \qquad \text{(II.7)}$$

The intensity of the local oscillator is much bigger than the scattered intensity.

In these conditions the autocorrelation function of the output signal of the photomultiplier, $S^H_{\text{exp}} \sim \langle I(t)I(0)\rangle$, for $t \neq 0$, is linearly related to the dynamical structure factor:

$$S^H_{\text{exp}}(\mathbf{K},t) = A_H + B_H S(\mathbf{K},t) \qquad \text{(II.8)}$$

where A_H and B_H are two time-independent parameters. With these techniques we observe correlation times ranging from about 10 μs to 1 s which corresponds to a maximum resolution of 10^{15}.

Now let us relax the hypothesis that we observe the scattered field on a point of the photocathode. We consider the whole surface of the photocathode. We state that the scattered field is coherent on an area called "coherence area", which is the diffraction pattern of the scattering volume.[8] If the surface of the photocathode has the dimensions of the "coherence area" we collect all the information given by light-scattering experiment and the expressions II.5 and II.8 can be applied.

The signal-to-noise ratio,[10] defined as $BS(\mathbf{K},0)/A^{1/2}$, being the determinant factor in the accuracy of the decay time of $S(\mathbf{K},t)$, we optimize this ratio. $BS(\mathbf{K},0)/A^{1/2}$ is proportional to the power light P_c scattered in a coherence area. P_c is related to the incident power light, P_i, and geometrical sizes of the scattering volume as follows:[8]

$$P_c \sim P_i\left(\frac{\partial n}{\partial c}\right)^2 \frac{\lambda_0^2}{a(\sin\theta + (a/L)|\cos\theta|)} \qquad \text{(II.9)}$$

$\partial n/\partial c$ is the refractive index increment of the polymer with respect to solvent. a and L are respectively the diameter and the length in the direction of the incident beam of the scattering volume. The signal-to-noise ratio can never exceed that obtained by collecting a single coherence area. In order to optimize the signal-to-noise ratio, focusing the incident beam, we reduce a to the minimum value compatible with a good definition of the scattering angle.

(b) Experimental Apparatus. The block diagram of the apparatus is given in Figure 2.

Light Source. The incident light is provided by an argon ion laser (λ 4.880 Å), with a light power ranging from 50 mW to 1 W. In order to avoid multiple scattering the light power value is chosen such that we have no visual turbidity. In some cases it was necessary to focus the beam in the sample.

Optical Detection. The arm of the spectrometer can be built in different fashions. We give here only one, which offers the advantage of switching rapidly from homodyne to heterodyne technique. By means of a mirror M_D and diaphragms D_1 and D_2 we collect the light scattered in a solid angle at an average angle θ. The focusing of the incident beam and the apertures D_1 and D_2 are adjusted in a such way that the signal-to-noise ratio is maximum without spread in the momentum transfert ($\delta\mathbf{K}/\mathbf{K} < 2\%$). The local oscillator is produced by taking a fraction of the transmitted beam, the intensity and polarization of which are adjusted by two polarizers A_1 and A_2.

Table II
Characteristics of the Macromolecules Used

M_w	M_n	M_w/M_n	M_z	R, cm	c^*, g/g
2.4×10^4 [a]	2.35×10^4	1.02	2.45×10^4	5.86×10^{-7}	2.26×10^{-1}
1.71×10^5 [a]	1.68×10^5	1.02	1.74×10^5	1.88×10^{-6}	4.85×10^{-2}
3.2×10^5 [a]	3.04×10^5	1.05	3.34×10^5	2.73×10^{-6}	2.96×10^{-2}
6.1×10^5 [a]	5.4×10^5	1.13	6.64×10^5	4.01×10^{-6}	1.79×10^{-2}
1.27×10^6 [b]				6.21×10^{-6}	1.00×10^{-2}
3.8×10^6 [a,b]		≤ 1.2		1.19×10^{-5}	4.25×10^{-3}
8.4×10^6 [b,c]				1.91×10^{-5}	2.28×10^{-3}
2.4×10^7 [c]				3.57×10^{-5}	9.99×10^{-4}

[a] In the dilute regime ($c < c^*$). [b] In the semidilute regime ($c > c^*$). [c] For the study of the internal motions ($KR \gg 1$).

After reflection on the mirror M_L and the beam-splitter B the local oscillator is mixed with the scattered field on the photocathode of the photomultiplier. By rotation and translation of the mirror M_L and beam-splitter B the spatial matching is ensured. In the case of homodyne detection the transmitted beam is trapped by a black screen.

Correlation. The correlation of the output signal of the photomultiplier can be performed in two ways. If the optical intensity at the photocathode is such that the delay time between two successive photoelectron pulses is bigger than 50 ns, we study the statistics of the photoelectrons with a digital correlator (Malvern). In the opposite case, i.e., with very high light flux, we built the autocorrelation of the photocurrent with an analogue correlator (Saicor).

(2) Sample Preparation and Characterization. In order to avoid degradation of the polymer samples the solutions (polystyrene–benzene) are made directly in the scattering cell and are not filtered. The monomer concentration is determined by weight with an accuracy better than 10^{-3}. The weight average molecular weight M_w and number average molecular weight M_n are obtained respectively by light scattering and osmotic measurements at the CRM of Strasbourg.[12] The z-average molecular weight M_z is calculated assuming that the number distribution is symmetrical

$$M_z = M_n(3 - 2\,(M_n/M_w)) \qquad \text{(II.10)}$$

The radius of gyration R is calculated from the expression

$$R = 1.45 \times 10^{-9} M_w^{0.595}\ \text{cm} \qquad \text{(II.11)}$$

found by light-scattering experiments.[12] The order of magnitude of the concentration c^* is obtained using the definition (eq 2)

$$c^* = \frac{1}{A\rho_B}\frac{M_w}{R^3} \qquad \text{(II.12)}$$

where ρ_B is the density of benzene ($\rho_B = 0.8794$ g/cm^3) and A the Avogadro number.[19]

In Table II we give the characteristics and the polydispersity of the samples used.

(3) Experimental Procedure. Dilute Range at $KR \ll 1$. The solution contains dust particles which fall by gravitation on the bottom of the cell. In the upper part of the sample we find a clean scattering volume. In this case homodyne detection with photon correlation has been used.

Semidilute Range at $K\xi \ll 1$. The high viscosity of the solution does not allow the dust particles to be eliminated from the scattering volume; they are homogeneously distributed in the sample cell. The light scattered by the dust acts as a local oscillator.[13] The ratio of the light scattered by dust to the light scattered by concentration fluctuations is unknown and therefore we are not sure that the conditions of heterodyning are respected. In order to be sure that these conditions are fullfilled we have added a local oscillator using the heterodyne spectrometer with two separated beams. The optical signal in this condition is very high and correlation of the output photocurrent of photomultiplier is made with the analogue correlator.

Dilute Range at $KR \gg 1$. The heterodyne spectrometer with two separated beams and the analogue correlator have been used. In this case the dynamical structure factor $S(\mathbf{K},t)$ is a complex function of time. With this method, we have a replica of the dynamical structure factor, independently of the field statistics.

(4) Numerical Analysis of the Experimental Autocorrelations. In every case the experimental autocorrelation is fitted to the theoretical time-dependent profile of the dynamical structure factor $S(\mathbf{K},\tau^{-1}(\mathbf{K})t)/S(\mathbf{K},0)$ by a least-squares three-parameter procedure.

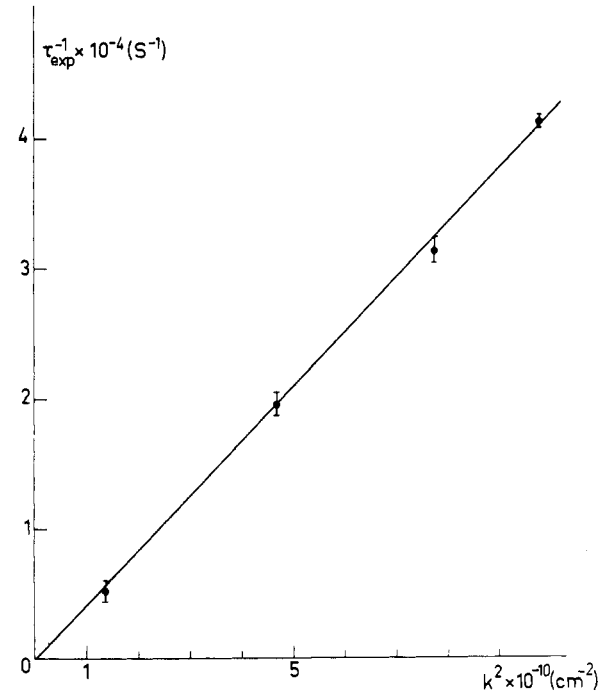

Figure 3. Inverse characteristic time of $S_{exp}(\mathbf{K},t)$ as a function of $\mathbf{K}^2$ in the dilute range. As homodyne detection has been used $\tau^{-1}{}_{exp} = 2\tau^{-1}$.

We minimize the quantity H^2

$$H^2 = \sum_{i=1}^{N}\left[S_{exp}(\mathbf{K},t_i) - A - B\left[\frac{S(\mathbf{K},\tau^{-1}(\mathbf{K})t_i)}{S(\mathbf{K},0)}\right]^X\right]^2 \qquad \text{(II.13)}$$

with respect to the parameters A, B, and $\tau^{-1}(\mathbf{K})$. X is equal to 1 for heterodyne detection and to 2 for homodyne detection. N is the number of experimental points.

For each fit we calculate the standard relative deviation V and the quality factor:

$$Q = 1 - \left[\sum_{i=1}^{N-1}\epsilon_i\epsilon_{i+1}\Big/\sum_{1}^{N}\epsilon_i{}^2\right] \qquad \text{(II.14)}$$

ϵ_i is the deviation of the ith experimental point from the corresponding calculated value.

Our empirical rule is that: the experimental curve can be represented by the chosen theoretical law and the determination of $\tau^{-1}(\mathbf{K})$ is meaningful if $V \leq 2\%$ and $Q \geq 0.7$.

III. Results and Discussion

In this section we describe and discuss the results obtained on different macromolecular weights M for different $\mathbf{K}$ and c values well within the regimes of Figure 1. We measure: three dynamical exponents α in dilute regime and β in semidilute regime for low kL values and γ in high kL regime (α, β, and γ are different from the corresponding theoretical values); the static exponent ν, when static lengths occur, which value is in agreement with theory and other static measurements.

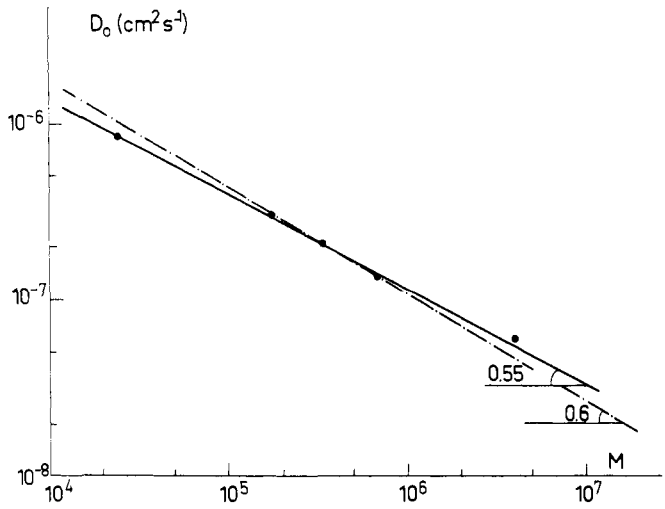

Figure 4. z-average molecular weight dependence of the diffusion coefficient at infinite dilution. The last point corresponds to M_w = 3.8×10^6 (z-average molecular weight of this polymer is unknown). The dotted line (-·-) is the theoretical prediction $D \sim M^{-0.6}$.

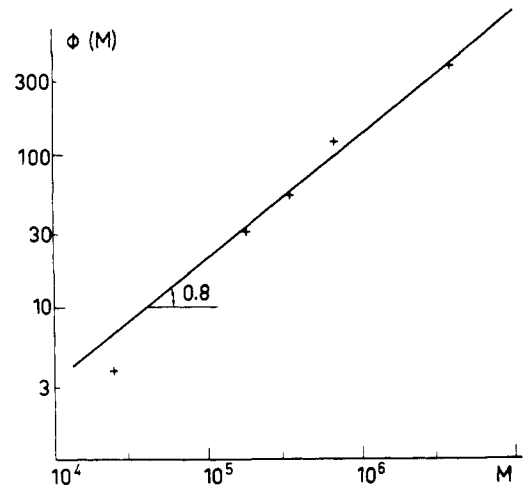

Figure 5. Variation of the concentration parameter $\phi(M)$ as a function of molecular weight. The dotted line scales like the theoretical law $M^{0.8}$.

In the discussion we use the static value of ν when geometrical lengths are considered and the α, β, and γ values when dynamical quantities occur.

(1) Dilute Regime $KR \ll 1$. The autocorrelation function of the scattered light has been studied as a function of concentration[3] for macromolecules of molecular weights ranging from 2×10^4 to 4×10^6 daltons. The autocorrelation function has an exponential profile; the inverse characteristic time of the dynamical structure factor is proportional to $\mathbf{K}^2$ (Figure 3)

$$\tau^{-1}(\mathbf{K}) = D(c,M)K^2 \qquad \text{(III.1)}$$

The effective diffusion coefficient $D(c,M)$ (determined with an experimental accuracy of 3%) obeys the relation:

$$D(c,M) = D_0(M)(1 + \phi(M)c) \qquad \text{(III.2)}$$

The mass distribution of the sample used is $M_w/M_n \leq 1.13$. As the experimental value of $D(c,M)$ is a "z-average" diffusion coefficient the quantities $D_0(M)$ and $\phi(M)$ have been plotted as a function of the "z molecular weight". $D_0(M)$, the translation diffusion coefficient in the limit of $c = 0$ (Figure 4), obeys the relation:

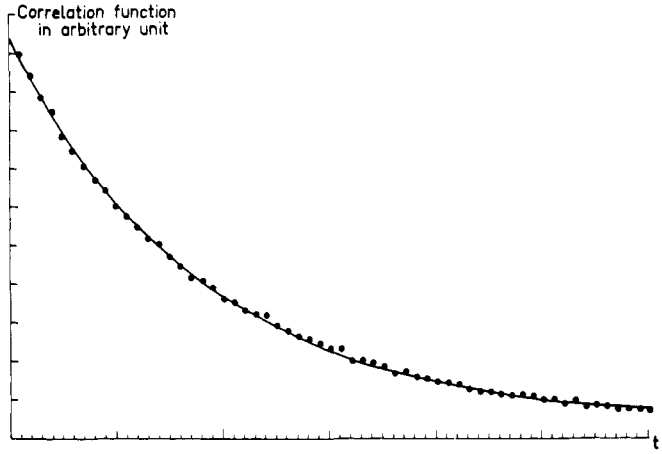

Figure 6. An example of correlation function $S_{exp}(\mathbf{K},t)$ observed in the pseudogel domain: (●) experimental points; (—) best fit using an exponentiel function. One interval in the time axis corresponds to 2.7 $\times 10^{-4}$ s

$$D_0(M) = (2.18 \pm 0.32) \times 10^{-4} M^{-\alpha} \text{ cm}^2 \text{ s}^{-1} \qquad \text{(III.3)}$$

$$\alpha = 0.55 \pm 0.02$$

The dynamical exponent α is different from the theoretical prediction but agrees with experimental results obtained from gradient concentrations:[14]

$$D_0(M) \sim M^{-0.54} \qquad \text{(III.4)}$$

The concentration dependence (eq III.2) of the diffusion coefficient reflects the interactions between coils and the molecular weight dependence of $\phi(M)$ is found to be $M^{0.8}$ (Figure 5). By a model of hard spheres taking into account geometrical consideration, it has been found[3,15] that the interaction between macromolecules is proportional to the volume occupied by the coils in the solution, c/c^*, which scales as $M^{3\nu-1}$. So we found experimentally that $\nu = 0.6$ and we conclude that the geometrical model of interaction is adequate.

In conclusion from these experiments in dilute solutions we have found that: (1) the diffusion coefficient D_0 is essentially mass dependent; (2) the hydrodynamical radius deduced from dynamical measurements is different from the geometrical radius of gyration

$$R_H \sim M^{\alpha} \qquad \alpha = 0.55 \pm 0.02 \qquad \text{(III.5)}$$

(3) the static exponent value ν is found to be 0.6 when geometrical values are observed.

(2) Pseudogel Domain. For this study, three molecular weights have been used (Table II). The concentrations investigated range from 1 to 10%, (with $c/c^* \geq 2.7$). For each sample the correlation time analysis of the scattered light is carried out in a wave vector range $\mathbf{K}$ such as $\mathbf{K}_{min} < \mathbf{K} < \mathbf{K}_{max}$ (see Figure 1). An example of the observed autocorrelation function is represented in Figure 6 with the exponential curve fitting (following expression II.13). The quality of the fit ($Q \simeq 0.8$) indicates that the dynamical structure factor is represented by a single exponential function of time. The inverse characteristic time of the dynamical structure factor is proportional to $\mathbf{K}^2$ (Figure 7) and the diffusion coefficient $D_g(c,M)$ is determined with an experimental accuracy of 5%.

The main consequence of the pseudogel model is that the diffusion coefficient increases with concentration like $c^{0.75}$ (eq I.11). The diffusion coefficient versus concentration is drawn in a log–log scale (Figure 8); D_g increases with concentration.

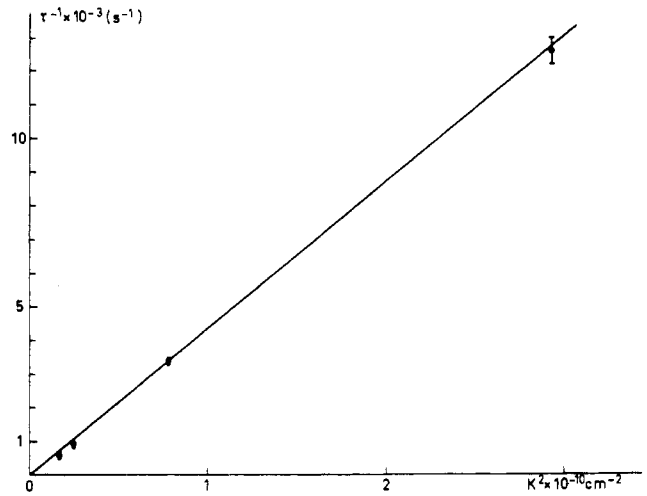

Figure 7. Inverse of the characteristic time of the dynamical structure factor as a function of the square transfer vector ($3\mathbf{K}_{min} < \mathbf{K} < 0.6\mathbf{K}_{max}$).

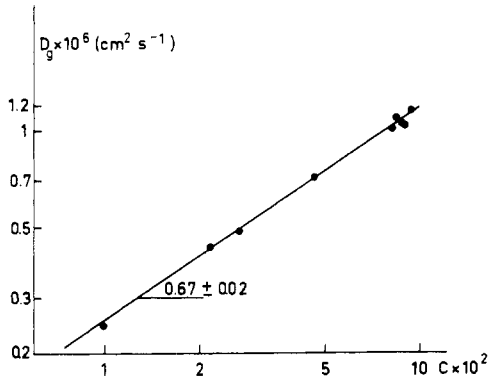

Figure 8. Diffusion in the pseudogel domain as a function of the concentration (log–log scale).

The straight line corresponds to:

$$D_g(c) = (5.63 \pm 0.16) \times 10^{-6} c^{\beta} \text{ cm}^2 \text{ s}^{-1} \qquad \text{(III.6)}$$

$$\beta = 0.67 \pm 0.02$$

The fact that $D_g(c)$ increases with concentration is in agreement with the theory. Again the experimental value of the dynamical exponent β does not match the theoretical value 0.75 derived from identification of static length with hydrodynamical length. The hydrodynamical length derived from (III.6) and (I.10) is:

$$\xi_H \sim c^{-\beta} \qquad \beta = 0.67 \pm 0.02 \qquad \text{(III.7)}$$

An important corollary of the pseudogel model is the molecular weight independence of the diffusion coefficient. To determine the mass dependence of D_g, three samples with approximatively the same monomer concentration but obtained from macromolecules with molecular weights 1.27×10^6, 3.8×10^6, and 8.4×10^6 daltons have been used. The results are reported in Table III. Within experimental error $D_g(c,M)$ is independent of molecular weight.[20]

Let us relate our results obtained in semidilute solutions to observations made in the dilute range. We can express the hydrodynamical length ξ_H as a function of the number of monomers $N(\xi)$ contained in a mesh of the polymer network. $N(\xi)$ is proportional to $c\xi^3$ where ξ^3 is the volume of the mesh. With the expression of ξ defined in eq 3, we derive:

$$N(\xi) \sim c^{1/(1-3\nu)} \qquad \text{(III.8)}$$

Table III
Diffusion Coefficients in the "Pseudogel" Domain for Different Molecular Weights at the Same Monomer Concentration

$M_w \times 10^{-6}$	$c \times 10^2$, g/g	$D \times 10^6$, cm² s⁻¹
1.27	8.71	1.05
3.8	8.68	1.06
8.4	8.38	1.09

Table IV
Inverse Characteristic Times as a Function of Momentum Transfer K at Large KR Values ($M_w = 24 \times 10^6$; $c = 5.54 \times 10^{-4}$)

KR	$\mathbf{K} \times 10^{-5}$, cm⁻¹	τ^{-1}, s⁻¹	$V \times 10^2$	Q
13.7	3.828	1.35×10^4	1.4	0.86
13.5	3.773	1.29×10^4	1.3	1
11.7	3.263	8.47×10^3	2.5	0.9
9.9	2.767	5.21×10^3	2	0.84
8.7	2.446	3.69×10^3	1.5	0.93
8.3	2.339	3.42×10^3	1.1	0.92
7.5	2.095	2.40×10^3	1.3	0.88
6.3	1.780	$1.42 \times 10^3$011.5	0.79	
4.4	1.241	5.32×10^2	1.5	0.82

With expression III.7 it follows:

$$\xi_H \sim N(\xi)^{(3\nu-1)\beta} \qquad \text{(III.9)}$$

Using the experimental value of β we found that:

$$(3\nu - 1)\beta = 0.536 \pm 0.016 \qquad \text{(III.10)}$$

Within the experimental error we find that the hydrodynamical length ξ_H scales as $N^{\alpha}(\xi)$ where α is the dynamical exponent found previously in dilute solution ($\alpha = 0.55 \pm 0.02$).

This point is in perfect agreement with observations of quasielastic light scattering in gel with permanent cross-links. Munch et al.[16] found in polystyrene network lightly cross-linked (swollen in benzene) that the diffusion coefficient D_g scales with the molecular weight of the mesh M, in the same manner as the diffusion coefficient at infinite dilution (expression III.4).

From these experiments we have shown that: (1) The diffusion coefficient is only concentration dependent[20] which indicates clearly that the coils form a network beyond c^*. (2) The hydrodynamical length ξ_H in semidilute solution and hydrodynamical radius R_H in dilute solution have the same scaling law with respect to the contour length.

(3) Internal Motions.[17] In order to test the theoretical predictions, high values of the product KR are required (region 3 in Figure 1). The two following samples have been used:

sample 1 $M_w = 24 \times 10^6$ daltons
sample 2 $M_w = 8.4 \times 10^6$ daltons

which correspond to $\mathbf{K}R_{max} = 13.7$ and $\mathbf{K}R_{max} = 7.2$, respectively.

We have no direct measurement of the polydispersity but we can assert that the polydispersity is unimportant if the translational diffusion coefficient $D_{exp}(c,M)$ measured agrees with the value $D_{ext}(c,M)$ extrapolated from data (section III.1) at lower monodisperse molecular weight. On sample 2 at $c = 9.51 \times 10^{-4}$ we measure

$$D_{exp}(c,M) = (5.5 \pm 0.4) \times 10^{-8} \text{ cm}^2 \text{ s}^{-1}$$

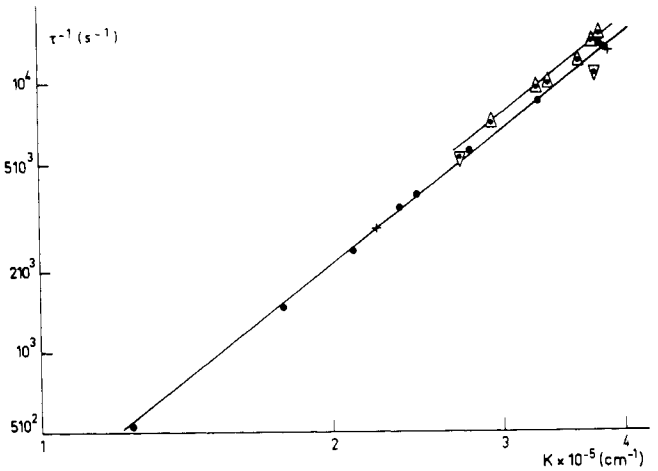

Figure 9. Log-log plot of the inverse characteristic time of the dynamical structure factor as a function of transfer vector at $\mathbf{K}R \geq 4.4$. $M_w = 8.4 \times 10^6$: (△) $c = 9.51 \times 10^{-4}$; (▽) $c = 8.56 \times 10^{-5}$. $M_w = 24 \times 10^6$: (●) $c = 5.54 \times 10^{-4}$; (+) $c = 1.67 \times 10^{-4}$.

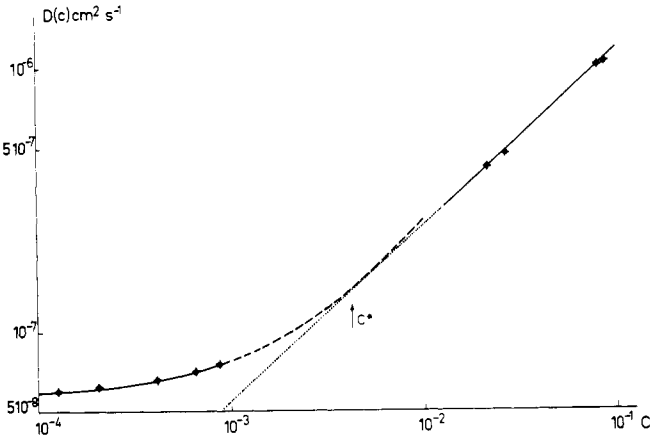

Figure 10. Diffusion coefficient as a function of concentration for the molecular weight 3.8×10^6 daltons: (◆) experimental points; (—) best fits for each regime; (- - -) and (···) extrapolations from each regime. We have reported the concentration c^* given in Table II.

and we calculate

$$D_{ext}(c,M) = 5.7 \times 10^{-8} \text{ cm}^2 \text{ s}^{-1}$$

We have fitted the data with eq I.21. Examples of this analysis are listed on Table IV. In the range $kR \geq 4.4$ the values obtained for the quality factor ($Q \sim 0.8$) indicate that the profile remains practically insensitive to the value of $\mathbf{K}$ when the condition $\mathbf{K}R \geq 4.4$ is fullfilled. Equation I.21 is therefore a meaningful model from which we have derived a characteristic time with an experimental accuracy of 5%. In Figure 9 the inverse characteristic times obtained with the two samples for various concentrations are plotted as a function of $\mathbf{K}$ on a log-log scale. We see that the characteristic time is slightly sensitive to the concentration. For $c \to 0$ the characteristic time is independent of the molecular weight, in good agreement with the theory.[20] The characteristic time behaves as:

$$\tau^{-1}(\mathbf{K}) \sim \mathbf{K}^{\gamma} \qquad \text{(III.11)}$$

The best determination of γ is

$$\gamma = 2.85 \pm 0.05 \qquad \text{(III.12)}$$

Now, using the intuitive argument developed in section I.2 (eq I.23) we deduce the variation of the diffusion coefficient $D(\mathbf{K})$ with the number of monomers, $N(\mathbf{K})$, contained within $\mathbf{K}^{-1}$. With $\tau^{-1}(\mathbf{K}) = D(\mathbf{K})\mathbf{K}^2$ we derive from eq III.11 that:

$$D(\mathbf{K}) \sim \mathbf{K}^{\gamma-2} \qquad \text{(III.13)}$$

Let us express this as a function of the number of monomers $N(\mathbf{K})$. Assuming that a subchain of size $\mathbf{K}^{-1}$ corresponds to a single chain with excluded volume we have $\mathbf{K}^{-1} \sim N^{\nu}(\mathbf{K})$ and

$$D(\mathbf{K}) \sim N^{\nu(2-\gamma)} \qquad \text{(III.14)}$$

The experimental value $\gamma = 2.85 \pm 0.05$ leads to:

$$D(\mathbf{K}) \sim N(\mathbf{K})^{-0.51 \pm 0.03} \qquad \text{(III.15)}$$

Within the experimental error this result is self-consistent with the results obtained in the other dynamical regimes. These experiments have shown that:

(1) At high values of $\mathbf{K}R$ and $c \to 0$ the inverse characteristic time is related to local properties (molecular weight independence[20]).

(2) For the $\mathbf{K}$ vectors investigated the hydrodynamic interactions are dominant in the internal motions of the polymer chain.

(3) The hydrodynamical length $\mathbf{K}_H^{-1}$ associated with a subchain of geometrical size $\mathbf{K}^{-1}$ scales with the number of monomers in the same manner as the hydrodynamical radius of the coil: $\mathbf{K}_H^{-1} \sim N^{0.51 \pm 0.03}(\mathbf{K})$.

IV. Continuity of the Characteristic Time between the Different Dynamical Regimes

So far we have analyzed the simple dynamical regimes far from the boundaries. Now let us examine the behavior of the characteristic times at the boundaries between the different asymptotic regions in order to test the scaling hypothesis.

(1) Between Dilute and "Pseudogel" Domain at $\mathbf{K}L \ll 1$. The behavior of the diffusion coefficient in the dilute range and the "pseudogel" domain, for a given molecular weight, is illustrated in Figure 10. We extrapolate the results obtained in the dilute regime toward the higher concentrations and in contrast we extrapolate the results obtained in the "pseudogel" domain toward the lower concentrations. The two curves are closed to each other at a concentration near the concentration c^* (see Figure 10). Thus we state that the diffusion coefficients must coincide at $c = c^*$. A scaling argument (section I.1.b) suggests that:

$$D_0(M) = D_g(c^*) \qquad \text{(IV.1)}$$

Using the expression of c^* (eq 2) and the experimental values we obtain the same result as previously mentioned, $\alpha = (3\nu - 1)\beta$, which is verified within the experimental error.

Thus, varying the concentration of the polymer solution we observe successively: at low concentrations, the polymer chains interact weakly and behave like spheres; at higher concentrations, the strong interactions between segments of the macromolecules lead to a medium which can be compared to a gel at a proper time scale.

(2) (a) Between Internal Motions and Diffusion Motion of the Coil. From previous experimental results in the asymptotic regions 1 and 3, at low concentrations, we know the $\mathbf{K}$ and M dependence of the inverse characteristic time of the dynamical structure factor.

At $\mathbf{K}R \ll 1$, the inverse characteristic time, associated with the diffusion of the coil, is essentially mass dependent and scales as $\mathbf{K}^2$:

$$\tau_0^{-1}(\mathbf{K}) \sim M^{-\alpha}\mathbf{K}^2 \qquad \alpha = 0.55 \pm 0.02 \qquad \text{(IV.2)}$$

At $\mathbf{K}R \gg 1$, $\tau_I^{-1}(\mathbf{K})$ which reflects the local properties of the chain is molecular weight independent and scales with $\mathbf{K}$ in the following manner

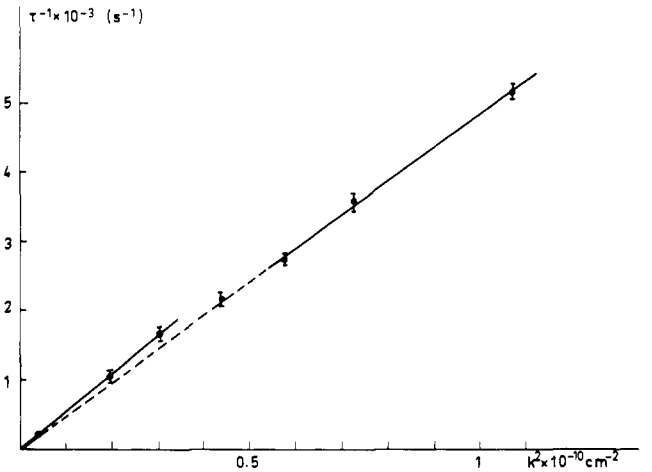

Figure 11. Inverse of the characteristic time of the dynamical structure factor as a function of the square transfer vector at $\mathbf{K} < \mathbf{K}_{min}$ and $\mathbf{K} > \mathbf{K}_{min}$ for a molecular weight of 1.27×10^6 at $c/c^* = 2.7$: (♦) experimental points; (—) best fit in each regime; (- - -) extrapolation from $\mathbf{K} > \mathbf{K}_{min}$.

$$\tau_I^{-1}(\mathbf{K}) \sim \mathbf{K}^\gamma \qquad \gamma = 2.85 \pm 0.05 \qquad \text{(IV.3)}$$

Now, let us make the supposition[17] that the inverse characteristic times $\tau_0^{-1}(\mathbf{K})$ and $\tau_I^{-1}(\mathbf{K})$ have the same order of magnitude at $\mathbf{K} = R^{-1} \sim M^{-\nu}$. We obtain the following relation:

$$M^{-\nu\gamma} \sim M^{-(\alpha+2\nu)} \qquad \text{(IV.4)}$$

Within the experimental accuracy the two exponent values $\gamma\nu$ and $(\alpha + 2\nu)$ are equal. This verifies the hypothesis and shows that the inverse characteristic time varies continuously from region 1 ($\mathbf{K}R \ll 1$) to region 3 ($\mathbf{K}R \gg 1$).

(b) Between Internal Motions and "Pseudogel" Motions. We suppose: (a) that the inverse characteristic time has the same dependence in the entire region 3; (b) a continuity requirement between τ_I^{-1} and τ_g^{-1} which are related to the internal motions and the cooperative diffusion of the pseudogel respectively at $\mathbf{K} = \xi^{-1} \sim c^{\nu/(3\nu-1)}$. Then we obtain a relation between exponents β and γ

$$\gamma = 2 + ([3\nu - 1]/\nu)\beta \qquad \text{(IV.5)}$$

With the value of β (= 0.67) and ν (= 0.6) we find $\gamma = 2.89$ in agreement with the experimental value. This last point verifies our hypothesis: the characteristic time related to the local properties has a uniform $\mathbf{K}$ dependence in the entire region 3.

Thus, by a variation of the wave vector it should be possible to observe the continuity of the dispersion relation associated with the characteristic time of the internal motions on one side and the pseudogel motions on the other side.

(3) Between "Pseudogel" and Translational Motions in Region 1' (Figure 1). The domain where the time scale of the observation is greater than T_R may be interpreted as the domain where translational diffusion motions of the chains are observable. The range of $\mathbf{K}$ vector such that $\mathbf{K} < \mathbf{K}_{min}$ is very narrow (see Figure 1). Therefore the extrapolation of the techniques used in region 1 is less appropriate (in this case, gradient concentration technique is a more convenient method). However, an experiment has been carried out in the proper wave vector domain for a molecular weight of 1.27×10^6 daltons and $c/c^* \sim 2.7$ (Table II). The inverse characteristic time is proportional to $\mathbf{K}^2$ (Figure 11) and the corresponding diffusion coefficient ($D_T = 5.4 \times 10^{-7}$ cm^2 s^{-1}) is in good agreement with the extrapolated value obtained from measurements in dilute range ($D = 5.33 \times 10^{-7}$ cm^2 s^{-1}). In Figure 11 we have also reported the inverse of characteristic time obtained in the pseudogel domain ($D_g = 4.83 \times 10^7$ cm^2 s^{-1} at $\mathbf{K} > \mathbf{K}_{min}$). The $\mathbf{K}$ value corresponding to the transition between macromolecular diffusion and pseudogel motion is $\mathbf{K}_{min} \simeq 6.7 \times 10^4$ cm^{-1}; this value has to be compared to the expected value derived from the theoretical expression of T_R (eq I.13 and I.14) ($\mathbf{K}_{min} \simeq 5.3 \times 10^4$ cm^{-1}).

This experiment indicates clearly that the network observed in region 1 has a finite lifetime. We are able to observe respectively a translational motion or a collective motion if the observation time is lower or bigger than T_R.

It should be interesting to measure the self-diffusion coefficient by any other appropriate method and determine the dependence of T_R upon molecular weight and concentration.

V. Conclusion

We have measured the characteristic time, τ, of the dynamical structure factor of the polystyrene dispersed in benzene as a function of the scattering angle and polystyrene concentration for several molecular weights.

We have determined the dynamical behavior of polymer solution in very different situations: diffusion of coils, internal motions of the chain, and cooperative diffusion of entangled polymer. In each of these situations we have found well-defined patterns of behavior. The characteristic times obey the following power laws:

(1) τ^{-1} is proportional to $\mathbf{K}^2$ and $M^{-0.55}$, in the limit of zero concentration and $\mathbf{K}R \ll 1$, as already known from earlier experiments.

(2) In the semidilute range at $\mathbf{K}\xi \ll 1$, τ^{-1} is proportional to $\mathbf{K}^2$ and $c^{0.67}$. What is remarkable is that the characteristic time depends only on the distance between the contact points which is a function of concentration only.

(3) For $\mathbf{K}R \geq 4.4$, the inverse characteristic time which is related to the deformation of the chain follows a simple dispersion relation $\tau^{-1} \sim \mathbf{K}^{2.85}$ and is independent of the molecular weight.

In the boundary regions the characteristic time varies continuously from one regime to another and scaling relations are respected. The dynamical exponents found in situation (2) and (3) can be explained if the hydrodynamical length scales with the dynamical exponent $\alpha = 0.55$ as a function of the number of monomers. Such a value of $\alpha = 0.55$ is different from the value predicted on the basis of identification between dynamic and static length. These data add to the unexplained exponent found in viscosity experiment and provide enough evidence for the necessity of a "dynamical" theory.

Acknowledgment. The authors gratefully thank J. des Cloizeaux and G. Jannink for stimulating discussions and P. G. de Gennes for suggesting the experiments.

References and Notes

(1) M. Daoud, J. P. Cotton, B. Farnoux, G. Jannink, G. Sarma, H. Benoit, R. Duplessix, C. Picot, and P. G. de Gennes, *Macromolecules*, **8**, 804 (1975).
(2) P. G. de Gennes, *Macromolecules*, **9**, 587 (1976).
(3) M. Adam and M. Delsanti, *J. Phys. (Paris)*, **37**, 1045 (1976).
(4) T. Tanaka, L. O. Hocker, and G. B. Benedeck, *J. Chem. Phys.*, **59**, 5151 (1973).
(5) For instance, P. J. Flory, "Principles of Polymer Chemistry", Cornell University Press, Itaca, N.Y., 1953.
(6) R. Pecora, *J. Chem. Phys.*, **40**, 1604 (1964).
(7) E. Dubois Violette and P. G. de Gennes, *Physics (Long Island City, N.Y.)*, **3**, 181 (1967).
(8) S. B. Dubin, Ph.D. Thesis, Massachusetts Institute of Technology, 1970.
(9) H. Z. Cummins and E. R. Pike, Ed., "Photon Correlation and Light-Beating Spectroscopy", Plenum Press, New York, N.Y., 1974.

(10) N. Ostrowsky, Thesis, Paris, 1970.
(11) C. Strazielle, private communication.
(12) D. Decker, Thesis, Strasbourg, 1968.
(13) M. Adam, M. Delsanti, and G. Jannink, *J. Phys. Lett.*, **37**, L53 (1976).
(14) R. N. Mukherjea and P. Rempp, *J. Chim. Phys. Phys.-Chim. Biol.*, **56**, 94 (1959).
(15) A. R. Altemberger and J. M. Deutch, *J. Chem. Phys.*, **59**, 894 (1973).
(16) J. P. Munch, S. Candau, R. Duplessix, C. Picot, and H. Benoit, *J. Phys. Lett.*, **35**, L239 (1974). See also R. Duplessix, Thesis, Strasbourg, 1975.
(17) M. Adam and M. Delsanti, *J. Phys. Lett.*, **38**, L271 (1977).
(18) See the determination of concentration dependence of ξ in the introductory section (eq 3).
(19) The concentration c in section I is expressed in monomer mass by unity volume (g/cm^3); in the other sections c is expressed in weight fraction (g/g).
(20) Thus polydispersity becomes unimportant in this domain.

Depolarized Rayleigh Dip Spectra in the *n*-Alkanes

G. D. Patterson* [1a] and G. R. Alms[1b]

Bell Laboratories, Murray Hill, New Jersey 07974, and the Department of Chemistry, Fordham University, Bronx, New York 10458. *Received June 9, 1977*

ABSTRACT: The existence of the depolarized Rayleigh dip in the spectra of two *n*-alkanes is clearly demonstrated. The spectra are found to be in good quantitative agreement with the general theories of depolarized Rayleigh scattering in viscoelastic media. The coupling parameter R is found to be 0.33 ± 0.02 for *n*-hexadecane at 65 °C and 0.38 ± 0.02 for *n*-docosane at 110 °C. Thus the *n*-alkane liquids are not qualitatively different from other liquids previously studied.

General theories[2-4] of Rayleigh scattering by a viscoelastic medium predict that the depolarized (I_{HV}) spectrum will exhibit a central dip when the quantity $q^2\eta/\rho$ is comparable to the overall half-width at half-height Γ_{HV} of the depolarized peak. The quantity $q = (4\pi n/\lambda)\sin\theta/2$ is the magnitude of the scattering vector for light of vacuum wavelength λ traveling in a medium with refractive index n and scattered through an angle θ in the scattering plane; η is the shear viscosity and ρ is the mass density. The dip is due to coupling between the hydrodynamic shear modes of the fluid and molecular reorientation. The predicted form of the spectrum is[2b]

$$I_{HV}(\omega) \propto \frac{\Gamma_{HV}}{\Gamma_{HV}^2 + \omega^2}\sin^2\theta/2 + \Gamma_{HV}\cos^2\frac{\theta}{2} \times \frac{(q^4\eta^2/\rho^2)(1-R) + \omega^2}{(\Gamma_{HV}(q^2\eta/\rho) - \omega^2)^2 + \omega^2(\Gamma_{HV} + (1-R)(q^2\eta/\rho))^2} \quad (1)$$

where R is a parameter which is equal to the fraction of the total shear viscosity which is due to coupling to molecular reorientation.

The theory should apply to any fluid composed of optically anisotropic molecules. The quantity $q^2\eta/\rho$ is known to be comparable to Γ_{HV} for the *n*-alkanes liquids. Thus, the central dip is predicted to occur if the coupling parameter R is sufficiently large. We expect any optically anisotropic liquid to show the dip feature provided the value of $q^2\eta/\rho\Gamma$ is in the range of ~0.1 to 0.7 and the value of R is sufficiently large (~0.1 or greater). However, a recent paper[5] by Champion and Jackson reported that none of the I_{HV} spectra in the *n*-alkanes showed any evidence of this central dip. The purpose of the present paper is to demonstrate the observation of a central dip in the depolarized Rayleigh spectra of two *n*-alkanes. The spectra were fit to the form given in eq 1 and a value of R was determined. The results are then discussed in detail and compared to the work of Champion and Jackson.

Experimental Section

The spectra were obtained as described previously.[6] The incident light was at 5145 Å and the free spectral range of the Fabry-Perot interferometer was 7.41 GHz. Great care was taken to render the incident light highly polarized in the horizontal direction relative to the scattering plane. The scattering angle was $\theta = 90°$. A Glan-Thompson polarizer was used to isolate the HV component of the scattered light.

The spectra were recorded with a 1024-point multichannel analyzer and fit with a nonlinear least-squares program described previously.[7] The deconvoluted values of Γ_{HV}, $q^2\eta/\rho$, and R for each spectrum were obtained by comparing the fitted results with spectra obtained by convoluting the instrumental function with eq 1.

n-Hexadecane (99%) and *n*-docosane (99%) were obtained from the Chemical Samples Co. The liquids were filtered directly into square quartz cells. The samples were held in a thermostated aluminum block and the temperatures were controlled to ±0.2 °C.

Results and Discussion

The depolarized (I_{HV}) spectrum of *n*-hexadecane at 65 °C is shown in Figure 1. The central dip is clearly visible. This feature was studied from 40–80 °C, but the best spectra were obtained near 65 °C. The overall width of the peak was Γ_{HV} = 1.30 ± 0.05 GHz and agrees quite well with the value reported by Champion and Jackson.[5] The quantity $q^2\eta/\rho$ calculated from direct measurements is 186 MHz for *n*-hexadecane at 65 °C. The value obtained from the fit to the depolarized spectrum is $q^{2\eta/\rho}$ = 196 ± 20 MHz. The coupling parameter is measured to be R = 0.33 ± 0.02. This value for R is in the same range as that measured in several previous studies of the depolarized Rayleigh dip in other liquids.[7-10] Although no dip was actually observed, Champion and Jackson estimated the value of R to be near 0.1 by comparing depolarized Rayleigh and flow birefringence data. The present results cast some doubt on the validity of that analysis.

The I_{HV} spectrum of *n*-docosane at 110 °C is shown in Figure 2. The overall width is Γ_{HV} = 1.05 ± 0.05 GHz. The calculated value of the shear width quantity is $q^{2\eta/\rho}$ = 187 MHz. The value obtained by fitting the spectrum is 199 ± 20 MHz. The coupling parameter is found to be R = 0.38 ± 0.02. The depolarized Rayleigh spectra of the *n*-alkanes are found to be in good quantitative agreement with the general theories.

The observation of the central dip feature in liquids depends on both physical considerations and experimental conditions. Keyes and Kivelson[3] have shown that no central dip exists when the quantity $q^2\eta/\rho\Gamma_{HV}$ is greater than a critical value given by

$$\left(\frac{q^2\eta}{\rho\Gamma_{HV}}\right)_C = \frac{(1-R)R + [(1-R)^2 + \tan^2\theta/2]^{1/2}R^{1/2}}{(1-R)^3 + \tan^2\theta/2} \quad (2)$$